Construction and Building Materials 253 (2020) 119062

Contents lists available at ScienceDirect

Construction and Building Materials

journal homepage: www.elsevier.com/locate/conbuildmat

A new viscoelastic micromechanical model for bitumen-filler mastic

Hassan Fadil [a], Denis Jelagin [a,*], Manfred N. Partl [a,b]

[a] Department of Civil and Architectural Engineering, KTH – Royal Institute of Technology Stockholm, Sweden
[b] Road Engineering/Sealing Components Laboratory, Empa – Swiss Federal Laboratories for Materials Science and Technology, Switzerland

HIGHLIGHTS

- A new finite element micromechanical modelling approach for mastics is proposed.
- The approach allows predicting the viscoelastic properties of mastic from its composition.
- Model predictions are validated with DSR measurements on four mastic materials.
- The measurements are performed in temperature interval from 0° to 10 °C for a wide range of filler concentrations.
- The proposed model captures the measured viscoelastic behaviour of mastic for the full range of material parameters examined.

ARTICLE INFO

Article history:
Received 18 December 2019
Received in revised form 2 April 2020
Accepted 5 April 2020

Keywords:
Mastic
FEM modelling
Micromechanics
Mineral filler
Rheology

ABSTRACT

A new micromechanical model for predicting viscoelastic properties of mastic is proposed and validated with experiments. The developed model is based on the finite element method and allows predicting the viscoelastic properties of mastic by means of the fundamental mechanical and geometrical properties of its constituents. The influence of modelling parameters on the model's accuracy is evaluated and optimal parameter combinations are identified. It is shown that the proposed model can capture the measured viscoelastic behaviour of mastics for the range of loading, temperature and material parameters examined. Accordingly, it may be a useful tool for optimizing mastics material design meeting the target viscoelastic properties.

1. Introduction

Asphalt mastic, defined as a combination of asphalt binder and mineral filler particles most of which passes the 63 μm sieve (EN 933-10), acts as a binding phase in asphalt mixture and accordingly, its influence on asphalt mixture properties is quite profound. This is particularly true in terms of fatigue, rutting and thermal fracture resistance properties of asphalt mixtures, cf. [1]. Understanding the mechanisms and parameters that control the rheological behaviour of mastic is thus crucial for ensuring adequate performance of asphalt mixtures. The present paper aims to contribute to this important topic by proposing and validating a new micromechanical modelling approach for predicting viscoelastic properties of bitumen-filler mastic, based on the finite element method (FEM).

Mechanical behaviour of bitumen-filler mastics has been and still is investigated experimentally, analytically and numerically by different research teams worldwide. In particular, physical, chemical and morphological properties of filler, i.e. its volumetric content, size distribution, shape, texture and surface area are known to govern the influence of filler on mastics, [2]. The void fraction in a dry-compacted mineral filler, also known as Rigden voids, was introduced by Rigden [3] as an important parameter having a significant influence on the mastic viscosity. As discussed e.g. by Guo et al. [4], Rigden voids represent a combined measure for the size distribution, shape, and texture of filler. Moreover, Rigden voids have a significant effect on the mastic's complex modulus [5]. In addition to the physical properties of the fillers, the physiochemical interaction between the filler and binder has an influence on the mastic's complex modulus [6]. This effect is attributed to the binder adsorption on the surface of the filler. The adsorption magnitude depends on the chemical composition of the mineral filler, i.e. the polar nature and specific surface area of the filler particles [7]. The filler properties have furthermore been reported to influence significantly fatigue and rutting performance

* Corresponding author.
E-mail addresses: hassanf@kth.se (H. Fadil), denis.jelagin@abe.kth.se (D. Jelagin), Manfred.Partl@empa.ch (M.N. Partl).

https://doi.org/10.1016/j.conbuildmat.2020.119062
0950-0618/

of mastics, e.g. [8–11]. In a study performed by the National Cooperative Highway Research Program (NCHRP) [1], 17 fillers from different sources in combination with 4 different asphalt binders were evaluated and it was emphasized that in addition to filler properties alone, the filler and binder combination is crucial to the performance of mastics and asphalt mixtures. From the studies above, it may be concluded, that there is strong experimental evidence that mastics rheological properties, as well as fatigue and rutting resistance, are highly dependent on its composition and on the properties of its constituents.

In order to account for the effect of mineral filler content on mastics rheology, several approximate analytical models have been proposed. In particular, the Generalized Self-Consistent Scheme (GSCS) [12,13] has been applied for obtaining the homogenised mechanical properties of particulate-reinforced composites. The GSCS has been applied on mastic by Buttlar et al. [6]. In order to account for the physiochemical stiffening effect, a concept of an equivalent rigid layer was introduced in their study. Buttlar et al. found that the modified GSCS is in reasonable agreement with the complex modulus of mastic measured at one frequency for the low and medium volume fractions of fillers; model deviations at higher volume fractions were attributed to the particle-to-particle interaction effects not accounted for adequately by analytical models. Yin et al. [14] conducted a comparative analysis of several approximate analytical models, for predicting viscoelastic properties of bitumen-filler mastic. The authors assumed rigid filler particles and incompressible binder and, based on comparison with the experimental measurements, they concluded that the self-consistent scheme gives more accurate predictions as compared to the other models examined. Yin et al. also pointed out, those assumptions of binder incompressibility and of rigid filler are not realistic if low-temperature properties of asphalt mastics are of interest. Ma et al. [15] compared three micromechanical analytical models considering inter-particle and physiochemical interaction. They concluded that the accuracy of all the models deteriorated as the filler volume fraction increased. At the same time, according to Ma et al. [15], the use of 4-phase model, accounting for the existence of both adsorbed and affected layers around the particles, resulted in somewhat better predictions at high filler concentrations. An alternative way to account for the effect of bitumen-filler physiochemical interaction has been proposed by Faheem and Bahia [5]. They presented a mastics stiffening model accounting for bitumen-filler interaction in terms of fundamental binder and filler properties. Model parameters were determined with multi-linear regression analysis of the complex modulus of mastics, measured for a range of filler types and concentrations. Hesami et al. [16] proposed an empirical framework accounting for the effect of filler particle-to-particle interactions on mastics viscosity at high temperatures. They showed that accounting for frictional interactions between filler particles allowed capturing fillers stiffening effects on mastics viscosity at high filler concentrations.

It has to be pointed out, that while the approximate analytical and empirical models summarized above allow evaluating mastics properties in a relatively simple way, they have several important limitations. As discussed above, particle-to-particle interaction effects are not fully captured in those models and accordingly, the models' accuracy deteriorates at high filler concentrations. Furthermore, filler size distribution and shape cannot be taken explicitly into account in analytical models. Hence the effect of those parameters on the performance of mastic may not be investigated quantitively. Finally, the validity of analytical models is limited to the cases of linear elastic and linear viscoelastic material behaviour. Thus those models may not be used to evaluate fatigue and plastic deformation performance of mastic. These shortcomings may be addressed by micromechanical numerical models, based on finite or discrete element methods. While 2D and 3D FEM have been used in several recent studies to evaluate mastics viscoelastic response, cf. e.g. [17,18], systematic validation of those models along with evaluation on how the various filler parameters influence mastics performance is still lacking. Accordingly, the goal of the present paper is to overcome these shortcomings by proposing and systematically validating a micromechanical FEM model for asphalt mastic.

This FEM micromechanical model is developed with a representative volume element (RVE) for mastics, where the filler phase is represented by randomly distributed elastic particles in a viscoelastic matrix. The filler phase in the material is generated with a robust and general particle generation procedure, based on the Large-scale Atomic/Molecular Massively Parallel Simulator (LAMMPS) open-source code. Periodic boundary conditions are used in mastics RVE modelling to reduce the model size and improve computational efficiency. The focus of this study is the capability of models to predict the shear relaxation functions, $G(t)$ of mastics. The influence of modelling parameters, in terms of RVE size, assumed bitumen's Poisson's ratio and filler size distribution on model accuracy is evaluated and discussed. In order to validate the model, bitumen-filler mastics variations are prepared with two different base binders and filler types. Mastic complex moduli are measured with the Dynamic Shear Rheometer (DSR) for a range of volumetric concentration of filler in temperature interval from 0° to 10 °C. A simple calibration procedure is proposed in order to capture the influence of the material parameters not explicitly accounted for by the model (such as adsorption and filler shape). By comparing the modelling results with experimental findings it is shown that the developed model can capture the viscoelastic properties mastics accurately for all materials and temperatures examined.

2. Problem formulation and computational modelling

Bitumen-filler mastic is a composite material consisting of at least two different phases: a base binder and embedded filler particles. Accordingly, the rheological behaviour of mastics depends on both binder and filler properties as well as on mastics composition. Provided that the strains are small and the damage is not an issue, the rheological behaviour of binders may be described by isotropic linear viscoelastic theory in tensor notation as follows:

$$s_{ij}(t) = \int_0^t G(t-\tau)\frac{d}{d\tau}e_{ij}(\tau)\cdot d\tau, \tag{1}$$

$$\sigma_{kk}(t) = \int_0^t K(t-\tau)\frac{d}{d\tau}\epsilon_{kk}(\tau)\cdot d\tau, \tag{2}$$

where $s_{ij} = \sigma_{ij} - \frac{1}{3}\delta_{ij}\sigma_{kk}$ and $e_{ij} = \epsilon_{ij} - \frac{1}{3}\delta_{ij}\epsilon_{kk}$ are the deviatoric stress and strain tensors, while σ_{kk} and ϵ_{kk} are the hydrostatic stresses and strains. $G(t)$ and K(t) represent the shear and bulk relaxation functions respectively. The generalised Maxwell model is used to describe the shear relaxation function of the binders:

$$G(t) = G_o - \sum_{i=1}^{N} G_i\left[1 - e^{-t/\tau_i}\right], \tag{3}$$

where N is the number of elements used to fit the equation, G_o is the instantaneous shear modulus, G_i is the Prony series element fitting parameter and τ_i is the relaxation time for the element. In order to obtain the Prony series parameters in Eq. (3), from the measured storage modulus $G'(\omega)$ of the binder, the Schapery and Park approximate interconversion method [19] is used. The method uses the

adjustment function λ' and the shear storage modulus $G'(\omega)$ as follows:

$$\lambda' = \Gamma(1-n)cos(\frac{n\pi}{2}), \tag{4}$$

$$G(t) \cong \frac{1}{\lambda'} G'(\omega)\Big|_{\omega=1/t}, \tag{5}$$

where n is the local slope in the log–log presentation of G' and ω, i.e. $n = \frac{dlog(G'(\omega))}{dlog(\omega)}$, and $\Gamma(x)$ is the gamma function $\Gamma(x) = \int_0^\infty e^{-k} k^{x-1} dk$. λ' gives the exact solution of Eq. (5) when $G'(\omega)$ can be described by a pure power law. The accuracy of this method deteriorates as the $G'(\omega)$ deviates from power law presentation

Filler particles may be represented as linear elastic isotropic material, with their behaviour defined by the two elastic constants: Young's modulus, E, and Poisson's ratio, ν. Presence of filler affects the rheology of mastic through mechanical and physio-chemical stiffening mechanisms. The present study is focused on fillers mechanical stiffening effect on the resulting viscoelastic properties of mastic. In order to come up with a robust computational procedure capable of capturing explicitly the effect of filler volume concentrationϕ and its size distribution on the resulting mastics properties, a micromechanical FEM model for mastics has been developed as described below.

Bitumen-filler mastics are represented as spherical isotropic elastic filler particles embedded into a dense viscoelastic binder matrix. The filler particles are characterized by a given size distribution and volume concentration. In this study, a perfect bonding is assumed between the filler and binder phases. Thus, the interface nodes are shared between the filler inclusions and the binder matrix. In order to limit the number of modelling parameters and due to experimental limitation, the effects of filler shape and of interface conditions are neglected in the present study. A suitable size for a representative volume element (RVE) for the model is determined based on the sensitivity study.

The filler particles are randomly distributed in the modelled mastic RVE, by using the particles dynamics simulator LAMMPS. The results of particle generation procedure are shown, along with the coordinate system used, in Fig. 1 (a) and (b) for particles of single size at $\phi = 10\%$ and for particles of multiple sizes at $\phi = 50\%$. Filler particles are generated, following a target size distribution, and placed randomly in a rectangular volume, having dimensions in the x_1 and x_3 coordinates equal to L (where L is the side length of the cubic RVE) and the dimension in the x_2 coordinate equal to 2L. Once all the particles are placed, the height of the volume is gradually reduced by moving the wall perpendicular to x_2 in the $-x_2$ direction, concentrating the spheres into a cubical volume with the RVE size. The particles are originally generated in LAMMPS with their sizes being about 5% larger than their targeted sizes. After the RVE is generated, the particle sizes are reduced to the target values and particle coordinates and diameters are transferred to the FEM software. In order to ensure that the filler phase construction procedure does not generate artefacts in terms of segregated particle distributions, average centre coordinates for each particle size are calculated. For all the models constructed in this study, the average particle coordinates were found not to deviate from centre more than 4% of the RVE size. Thus, reasonably indicating uniform filler distributions in the models. This is done to ensure that all the generated particles are embedded in the binder matrix and not in direct contact with each other. The assumption is that the particles are not in direct contact with each other implies that all filler particles are fully coated by bitumen and particle agglomeration does not happen. This method allows generating a filler phase with a given size distribution and to achieve high volumetric concentrations, i.e. at least ϕ =60% for single size spheres with maximum concentrations increasing for multi-size particle distributions. The same procedure can be followed to generate ellipsoidal particles. The resulting FE model of mastic is illustrated in Fig. 1(c), for the case of bitumen filler mastic with 10% of filler.

In order to investigate the effect of the mastic composition on its linear viscoelastic behaviour, a virtual uniaxial test on mastic is performed and the homogenised properties of mastic are obtained as follows. In order to reduce the size of the RVE modelled, and for improving the computational efficiency, periodic boundary conditions (PBCs) are employed. In this approach, the boundary conditions (prescribed displacements or tractions) are chosen such as to cause the same average strain or stress within a homogeneous material of the same size as the RVE. As discussed by e.g. Gitman et al. [20], using PBC allows to significantly reduce the size of the model without compromising the accuracy. In particular, use of PBC significantly reduces the effect of the model's shape and size on the results, as the model represents an infinite volume of the material with periodically repeated internal structure. For the coordinate system shown in Fig. 1(c) the PBCs in terms of displacements, $u(x_1, x_2, x_3)$, are defined as follows [21]:

$$u(x_1, x_2, 0) - u_3 = u(x_1, x_2, L), \tag{6}$$

$$u(x_1, 0, x_3) - u_2 = u(x_1, L, x_3), \tag{7}$$

$$u(0, x_2, x_3) - u_1 = u(L, x_2, x_3), \tag{8}$$

where u_1, u_2 and u_3 are the displacements in the x_1, x_2 and x_3 directions. In this study, uniaxial tension tests on mastics are simulated

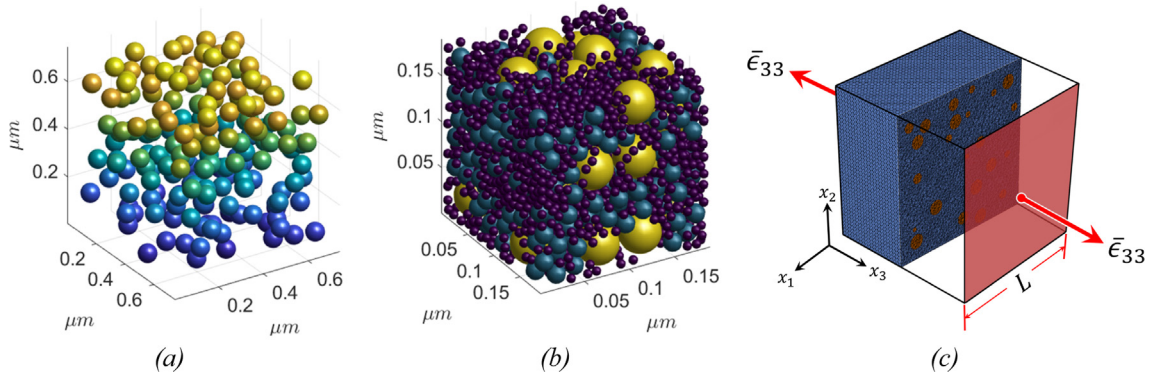

Fig. 1. generated filler particles with ϕ= (a) 10% single size, (b) 50% with multiple sizes and (c) FE model of the mastic with the 10% of filler particles.

by applying an average strain $\bar{\varepsilon}_{33}$ to the model, i.e. $u_3 = \bar{\varepsilon}_{33}L$. The following boundary conditions are applied on the free specimen sides:

$$\int_{S_{RVE}} t_{x_1} dS_{RVE} = 0, \tag{9}$$

$$\int_{S_{RVE}} t_{x_2} dS_{RVE} = 0, \tag{10}$$

where t_{x_1} and t_{x_2} are the tractions for the opposing RVE surfaces S_{RVE} that are perpendicular to the x_1 and x_2 coordinate axes, i.e. S_{RVE} with the coordinates $(0, x_2, x_3)$, (L, x_2, x_3), $(x_1, 0, x_3)$ and (x_1, L, x_3). It has to be emphasized, that the use of PBCs defined by Eqs. (6)–(10), results in a model of RVE, imbedded in infinitely large material with the periodically repeated internal structure. Thus, the rectangular element shown in Fig. 1 only controls the periodicity of the internal structure and not the numerical specimen size and shape.

A periodic mesh is generated in the Abaqus 6.14 FEM software, using the HOMTOOLs plug-in, developed by Lejeunes and Bourgeois [22]. The nodes on opposing faces of the model are linked by the coupling Eqs. (6)–(8). HOMTOOLS was also used to automatically extract the volume average strains and stresses from the corresponding local quantities according to:

$$\bar{\varepsilon}_{ij} = \frac{1}{|V_{RVE}|} \int_{V_{RVE}} \varepsilon_{ij} dV_{RVE}, \cdot \bar{\sigma}_{ij} = \frac{1}{|V_{RVE}|} \int_{V_{RVE}} \sigma_{ij} dV_{RVE} \tag{11}$$

where $\bar{\varepsilon}_{ij}, \bar{\sigma}_{ij}$ and ε_{ij}, σ_{ij} are volume average and local stresses and strains respectively [23].

An average strain of $\bar{\varepsilon}_{33} = 2\%$ is applied to the numerical model at the beginning of the simulation and maintained for 400 s, i.e.:

$$\bar{\varepsilon}_{33}(t) = 2\% \times H(t = 0). \tag{12}$$

The uniaxial tensile loading condition is used due to the the fact that uniaxial loading is less sensitive to material periodicity as compared to shear loading when PBC are utilised, cf. [20]. Therefore, for the same RVE size, the uniaxial tensile loading condition is expected to provide results that are closer (as compared to other loading modes) to the assumed isotropic behaviour. As the loading case defined by Eq. (12) results in a time independent strain in the loading direction, Poisson's ratio dependence on the memory effect is eliminated, cf. Hilton [24]. Accordingly, Hooke's law, combined with the viscoelastic correspondence principle, can be used to obtain the required viscoelastic material properties.

The homogenized viscoelastic Poisson's ratio, $\bar{\nu}(t)$, and relaxation function $\bar{E}(t)$ of the RVE are calculated based on the volume average of the transverse strains $\bar{\varepsilon}_{11}(t)$ and $\bar{\varepsilon}_{22}(t)$ and uniaxial stress $\bar{\sigma}_{33}(t)$, obtained from the model:

$$\bar{\nu}(t) = -\frac{\bar{\varepsilon}_{11}(t) + \bar{\varepsilon}_{22}(t)}{2\bar{\varepsilon}_{33}(t)}, \tag{13}$$

$$\bar{E}(t) = \frac{\bar{\sigma}_{33}(t)}{\bar{\varepsilon}_{33}(t)}. \tag{14}$$

$\bar{G}(t)$ is obtained from $\bar{E}(t)$ and $\bar{\nu}(t)$ by using the viscoelastic correspondence principle from the elastic relation:

$$G = \frac{E}{2(1+\nu)}, \tag{15}$$

$$s \times G(s) = \frac{s \times E(s)}{2(1 + s \times \nu(s))}, \tag{16}$$

where $f(s)$ is the Laplace transform of the function $f(t)$. As pointed out above, Eq. (16) is strictly applicable only to the loading cases where the strain is applied instantaneously such as the case in Eq. (12), i.e. to class II Poisson ratio according to Hilton [24].

$$f(s) = \mathcal{L}\{f(t)\} = \int_0^\infty f(t) \times e^{-st} dt. \tag{17}$$

$\bar{G}(t)$ is then obtained by performing the inverse Laplace transform on Eq. (17). $\bar{G}(t)$ obtained from the simulations may then be converted to $G^*(\omega)$ of mastic by using the Prony series based conversion method proposed by Park and Schapery [25]. It has to be pointed out, that as linear viscoelastic analysis is performed, the obtained homogenised viscoelastic properties are independent of the magnitude of the imposed strain in Eq. (12).

To summarize, the FEM modelling approach presented above allows for obtaining $\bar{G}(t)$ of the mastic from its material parameters and composition. In particular, the following parameters are incorporated explicitly into the model: viscoelastic properties of binder phase properties, $K(t), G(t)$, elastic properties of filler, E, υ, as well as the size distribution and volume concentration ϕ of the filler. In the following section, experiments performed in order to obtain the input parameters for the model as well as to validate the model are summarized and discussed.

3. Experimental investigation

For experimentally investigating the effect of the mastic's material parameters on its rheological behaviour, mastics specimens were prepared as described below. The filler concentrations and types, as well as the binder materials, were chosen for the experimental study to cover a wide range of resulting mastics properties. The mastics samples were prepared using two different binders supplied by Nynas AB: neat bitumen with a 70/100 PEN, softening point of 46 °C and with kinematic viscosity of 235 mm^2/s at 135 °C [26], and SBS Polymer Modified Bitumen (PmB), commercially available from Nynas AB with a 40/100 PEN and softening point of 75 °C [27]. With each binder, two different fillers were used (i) hydrated lime, $Ca(OH)_2$, and (ii) quartz sand, resulting in a total of four different mastics materials.

The densities and Rigden voids (RV) of the fillers are shown in Table 1. They were determined using pycnometers according to ISO standard ISO 1183-1:2012 and a Rigden apparatus according to Swedish Standard SS-EN 1097-4:2008 respectively. As seen in Table 1, RV values for the two fillers used differ by approximately a factor of 2, indicating that the fillers examined have a very different morphology. The high RV value for hydrated lime filler may be attributed to the shape of the particles, texture, size distribution and porosity, as discussed by e.g. Lesueur et al. [28] and Antunes et al. [29].

The size distribution of the fillers' particles was measured using a laser diffractometer (Mastersizer 3000), with water and ethanol as dispersion mediums for the quartz sand and hydrated lime fillers respectively. The measured volume distributions of the particles sizes are shown in Fig. 2(a), where it is seen that the quartz sand has larger particles as compared to hydrated lime. The shaded regions in Fig. 2(a) highlight the central portions of the size distribution curves corresponding to 75% of the filler volume; these regions cover the sizes ranges 2.42–27.40 μm and 5.92–51.80 μm for hydrated lime and quartz sand respectively. For computational

Table 1
Density and Rigden voids of the fillers with a 95% confidence interval.

Property/Material	Hydrated Lime	Quartz Sand
Particle Density (g/cm^3)	2.378 ± 0.055	2.687 ± 0.021
Rigden Voids (%)	64.79 ± 1.44	34.00 ± 2.35

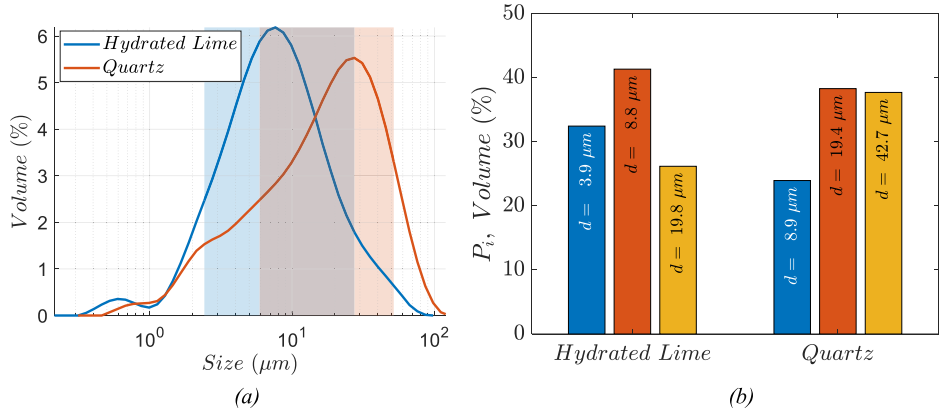

Fig. 2. Filler particles size distributions (a) measured, (b) simplified size distributions used in the modelling, d is the diameter of the particle.

efficiency, only particles in the 75% volume range are modelled explicitly in the FEM models of mastic. The simplified size distributions of the particles used in the models are shown in Fig. 2(b).

In order to characterize the viscoelastic properties of the two binders, their complex moduli, $G^*(\omega)$, and phase angles, $\delta(\omega)$, were measured with the DSR. Frequency sweep tests were performed for $\omega = 0.0628 - 62.8\ rad/s$, at temperatures of 0 °C, 5 °C and 10 °C according to EN-14770. Two replicates of each material were tested observing differences between the results below 20%. Measurement results, transformed to the reference temperature of $T_{ref} = 0$ °C, are presented in Fig. 3. The master-curves in Fig. 3, were constructed assuming that the shift factors (a_T) follow the Williams–Landel–Ferry equation:

$$log(a_T) = -\frac{C_1(T - T_{ref})}{C_2 + (T - T_{ref})}, \tag{18}$$

where T is the measurement temperature and C_1 and C_2 are fitting constants, resulting in an optimal fit of the measurements results, shifted to the reference temperature. The obtained $G^*(\omega)$ master curves were fitted with the following sigmoidal function:

$$G^*(\omega) = \delta + \frac{\alpha}{1 + e^{\beta - \gamma[log(\omega) - log(a_T)]}}, \tag{19}$$

where δ, α, β and γ are the sigmoidal function constants, determined through nonlinear regression. The same shift factors generated for the $G^*(\omega)$ master curves are used to create the phase angle ($\delta(\omega)$) master curves presented in Fig. 3. As seen in Fig. 3 the PmB has a somewhat lower complex modulus and higher phase angles at the temperature interval examined. Similar observations have been presented by Airey [30], where the complex modulus for one type of neat bitumen became higher than for PmB at high frequencies and low temperatures.

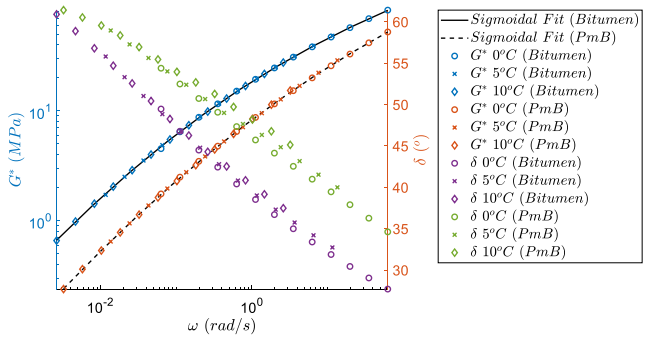

Fig. 3. Master-curves for bitumen and PmB at $T_{ref} = 0$ °C.

Based on the results presented in Table 1, Figs. 2 and 3, it may be concluded that the binders and fillers used in this study represent different conditions with respect to filler size distributions and morphology as well as binders viscoelastic properties. Furthermore, as discussed in previous studies, e.g. [6,7], in case of hydrated lime filler, its chemical reactivity may affect the resulting rheology of bitumen-filler mastics. In the present study, the fillers were mixed with the binders to the volume concentrations $\phi =$ 10%, 20% and 30% for hydrated lime filler, and $\phi =$ 10%, 30% and 50% for quartz sand. Those filler concentrations were chosen in order to have mastics samples covering a wide range of volumetric concentrations from a relatively low value of $\phi =$ 10%, to the ones close to the critical volume fractions of the fillers, $\phi_c = 1 - RV$. Using this equation and Rigden voids values presented in Table 1, ϕ_c values were calculated as 35.21% and 66.00% for hydrated lime and quartz sand respectively. The mass of filler m_f, corresponding to the target volume concentrations ϕ, was determined based on the measured density of the filler ρ_f, and with the densities of the binders, taken as $\rho_b = 1$ g/cm^3 following the producer's datasheets.

$$\phi = \frac{v_f}{v_f + v_b} = \frac{m_f/\rho_f}{m_f/\rho_f + m_b/\rho_b}, \tag{20}$$

where V_f and V_b are the volumes of filler and binder respectively and m_b is the mass of the binder.

For preparing the mastics, the binders were pre-heated for two hours at 164 °C. The filler was added gradually to the binder during mixing with a mechanical mixer at 164 °C. The mastics were distributed into small metallic containers and each of them was reheated and used for one DSR test to ensure similar thermal histories between the tests. For the rest of the study, the mastics tested were labelled as follows: (1) BL for neat bitumen and hydrated lime, (2) BQ for neat bitumen and quartz sand, (3) PL for polymer-modified bitumen and hydrated lime and (4) PQ for polymer-modified bitumen and quartz sand. The volumetric filler content is indicated with a number following the letters, i.e. BL10 denotes mastic with a neat bitumen binder and 10% hydrated lime filler.

$G^*(\omega)$, and $\delta(\omega)$ of the prepared bitumen-filler mastics samples were measured with the DSR and the 8 mm parallel plate setup. In order to ensure that the measurements were performed in the linear viscoelastic range (LVE), strain sweep tests were performed on each mastic material at 5 °C and at a frequency of 1.59 Hz. It has been found that for all the materials tested, the measured G^* does not change more than 5% for the strains below 0.2%. Accordingly, a strain of 0.2% was used in the frequency sweep tests performed in the frequency range from 0.1 Hz to 10 Hz, and at $T = 0$ °C, 5 °C and

10 °C according to EN-14770. Two replicates were tested in the frequency sweep tests for each mastic type. The difference between the two measurements performed on the same mastic type was found to be less than 20% for all the materials examined. Based on DSR measurements, master-curves were constructed for each material, at a $T_{ref} = 0$ °C, using the Eq. (18).

4. Computational study

Mastic models are developed for all binder and filler combinations tested. The volumetric mastic compositions and the measured properties of its constituents are incorporated in FEM modelling as follows. Filler particles are generated to attain the target value of ϕ and the size distributions presented in Fig. 2(b). For both filler types, a spherical particle shape is assumed in numerical modelling, cf. Fig. 1(b). The number of spheres of each diameter, d_i, with the corresponding volume, V_i, reads:

$$N_i = \frac{V_{RVE} \cdot P_i \cdot \phi}{V_i} \tag{21}$$

where N_i is the number of particles of i size, V_{RVE} is the volume of the RVE, P_i is the volume percentage of the particle size i from the total particles volume and ϕ is the volume fraction of the filler in the mastic. The filler particles were assumed to have properties like crystalline quartz, $E = 70$ GPa and $\nu = 0.17$ [31]. The viscoelastic matrix properties were determined from the DSR measurements reported in Fig. 3. The DSR measurements have been converted into relaxation moduli $G(t)$ with the Eqs. (4) and (5); the parameters for the Prony series fit of $G(t)$ are shown in Table 2. The bulk modulus, $K(t)$, was assumed to be constant for both binders and taken to be equal to the value reported by Wolf [32] for bitumen at 0 °C. It has to be pointed out that the measurements reported in [32] do not necessarily reflect the binders used in this study. The assumption of constant $K(t) = 344.8$ MPa results, however, in an instantaneous Poisson's ratio $\nu_o = 0.48$, $\nu(t)$ which increases asymptotically to 0.5 with loading time. This also agrees well with the value of ν_o at 0 °C reported by Maillard et al. [33] and with the values measured in [34] for bitumen with penetration grade 50/70. The assumed $K(t)$ seems thus to be reasonably realistic.

In order to establish model size representative for the macroscale properties of the mastic, i.e. an RVE size, a sensitivity study has been performed. As defined by Hill [23], RVE should contain a sufficient number of inclusions for obtaining computed properties that are independent of the surface displacements and tractions. In a sensitivity study, four models of RVE were created at $\phi = 30\%$, and with a single size of filler particles. All the models had a cubic shape with a side length, $L = 5$, 7.5 and 10 times the diameter of the filler particles. It has been observed that the effect of L on the calculated $G(t)$ of mastic diminishes quickly with the increasing model size. In particular, the difference in $G(t)$ calculated with the model sizes of 7.5 and 10 times the particle size was found to be within 3%. Accordingly, the model size was kept at 10-times the diameter of the filler particles in all subsequent models.

Models were meshed in ABAQUS using the built-in tetrahedral mesh generator. The element type used for the filler particles was the quadratic tetrahedral element of type C3D10 (10 degrees of freedom). In order to avoid volume locking associated with nearly incompressible materials, the hybrid elements of type C3D10H (11 degrees of freedom) were used for the binder matrix. Element sizes were chosen based on the mesh sensitivity analysis. The approximate global element size, L_{mesh}, was set to $0.05L$, while the minimum size of elements was allowed to reach $0.34L_{mesh}$. In the sensitivity analysis performed at different L_{mesh}, it was found that decreasing the mesh size below 0.05L results in less than 5% change in the calculated $G(t)$ of mastic.

In order to examine the effect of a constant bulk modulus assumption on the results, a brief parametric study has been performed as follows. $G(t)$ for mastic, containing single size spherical filler particles at $\phi = 30\%$, has been calculated assuming different types of volumetric behaviour for the binder, namely $K(t) = 344.8$ MPa and three cases of constant Poisson's ratio, $\nu(t) = 0.2, 0.4, 0.5$, i.e. assuming a constant ratio between the $G(t)$ and $K(t)$. In Fig. 4, the effect of the assumed volumetric behaviour of the binder phase on the stiffness ratios $G_{mastic}(t)/G_{bitumen}(t)$ is examined. The stiffening ratios in Fig. 4 are obtained based on the $G_{mastic}(t)$, calculated from the model and $G_{bitumen}(t)$ from Table 2. As seen in Fig. 4, the assumed volumetric behaviour may significantly affect the results. The stiffening ratios calculated for $\nu(t) = 0.4$ and 0.2 and $K(t) = 344.8$ MPa differ with a maximum of 30% and the difference between the cases is approximately constant for the time interval examined. At the same time, for the case of $\nu(t) = 0.5$, the calculated stiffness ratios show distinctly different behaviour. The difference between the $K(t) = 344.8$ MPa and $\nu(t) = 0.5$ cases changes with the loading time, starting with 15% difference at $t = 0.01\,s$ and reaching approximately 550% at $t = 400\,s$. Thus, it may be concluded that the assumed volumetric behaviour of the binder phase may have a profound effect on the calculated $G(t)$ of mastics. In this context, assuming constant $K(t)$ appears to be more justifiable, based on the previous studies [35].

The mastics models described above incorporates explicitly the mechanical properties of binders and fillers as well as the influence of the filler size distribution. At the same time, certain important parameters which may affect viscoelastic properties of mastic are not accounted for in the actual model. In particular, filler shape and texture, as well as possible physiochemical interactions between bitumen and filler, are not modelled presently, but they

Table 2
Prony series fitting parameters for the binders.

Element	g_i(Neat Bitumen)	g_i(PmB)	τ_i(seconds)
0	160.8156 (MPa)	128.3926 (MPa)	0
1	0.1621	0.2575	0.0010
2	0.2670	0.3040	0.0036
3	0.1898	0.1790	0.0132
4	0.1440	0.1177	0.0479
5	0.0990	0.0689	0.1741
6	0.0640	0.0383	0.6325
7	0.0375	0.0191	2.2974
8	0.0202	0.0091	8.3453
9	0.0097	0.0038	30.3143
10	0.0042	0.0016	110.1169
11	0.0019	0.0007	400.0000

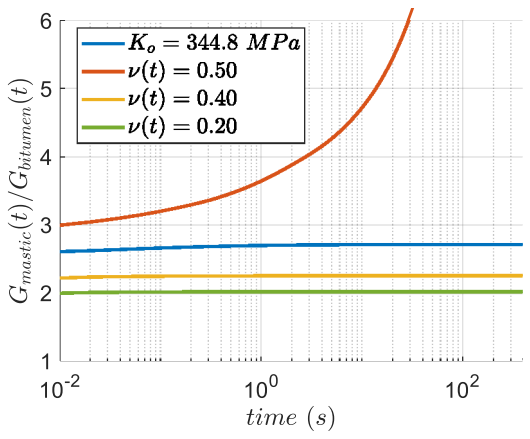

Fig. 4. Mastic to bitumen stiffening ratios at different bitumen's Poisson's ratios.

are known to influence the rheology of the mastics significantly, cf. [6,7]. In order to account for those factors, at least partially, a simple calibration procedure is implemented as described below.

It is assumed in this study that effects of filler shape and of the adsorbed layer around the particle on the viscoelastic properties of mastic may be accounted for by adjusting the volumetric filler concentration in the material. Accordingly, a calibration factor C_v is introduced, allowing to adjust the volume fraction of the filler to its effective value ϕ_e:

$$\phi_e = C_v \cdot \phi \tag{22}$$

In order to identifyC_v, FEM simulations are performed for each mastic material at $\phi = 10–60\%$ with 10% steps, as well as $\phi = 65\%$, and mastic responses in terms of complex moduli, $G^*_{FEM}(\omega, \phi)$, are recorded over a range of ω and ϕ. The obtained $G^*_{FEM}(\omega, \phi)$ is then fitted at each frequency ω_i by the following equation:

$$G^*_{FIT}(\omega_i, \phi) = a_i \cdot e^{b_i \times \phi} + c_i \cdot e^{d_i \times \phi} \tag{23}$$

where a, b, c and d are fitting parameters, obtained with non-linear regression as follows:

$$Min \left| \left(\frac{G^*_{FIT}(\omega_i, \phi) - G^*_{FEM}(\omega_i, \phi)}{G^*_{FEM}(\omega_i, \phi)} \right)^2 \right| \tag{24}$$

The two-term exponential function used in Eq. (23) was tentatively chosen as a fitting function, as it allows for capturing two stiffening regimes for mastics. Namely, diluted and concentrated regimes, cf. e.g [5,16]. $G^*_{FIT}(\omega_i, \phi)$ was found to capture the model results well, with $R^2 > 0.99$ for all materials, ω and ϕ values evaluated.

The models are calibrated then by identifying a single C_v value for each binder-filler combination. C_v is identified by minimizing the difference between the $G^*_{FIT}(\omega_i, \phi_e)$ and the experimental measurements, $G^*_{DSR}(\omega_i, \phi)$, for all the frequencies and filler concentrations examined:

$$Min \sum_{\phi_i=\phi_{min}}^{\phi_{max}} \left| \sum_{\omega_i=\omega_{min}}^{\omega_{max}} \left(\frac{G^*_{FIT}(\omega_i, \phi_e) - G^*_{DSR}(\omega_i, \phi_i)}{G^*_{DSR}(\omega_i, \phi_i)} \right)^2 \right|. \tag{25}$$

C_v is then calculated from ϕ_e by using Eq. (22). Once C_v is determined, FEM models are set up to capture the response of the mastic at effective filler concentration, defined by Eq. (22). The calibration procedure is summarised as a flowchart in Fig. 5.

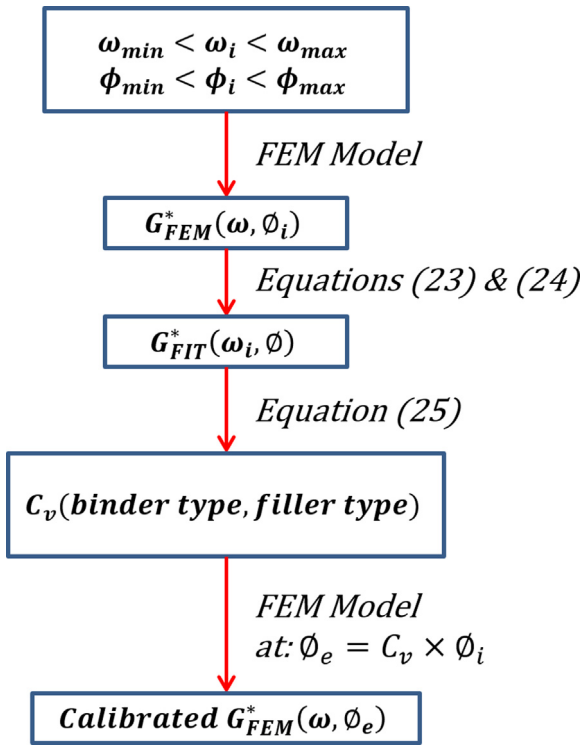

Fig. 5. Flowchart for the calibration procedure between the FEM model and the experiment.

5. Results and discussion

In what follows, the capabilities of the developed model in terms of predicting viscoelastic properties of mastic are examined. First, results from a brief numerical parametric study are presented in order to compare the developed model with the available analytical solution as well as to evaluate the effect of filler size distribution on mastic. Later, the attention is focused on the evaluation of the model's capability to capture the viscoelastic response of mastic specimens measured with the DSR.

5.1. Parametric study

In Fig. 6(a) and (b), the distributions of the strains in the loading direction ε_{33} in the mastics with a bitumen binder and quartz sand filler are shown in Fig. 6(a) for $\phi = 10\%$ and in Fig. 6(b) for $\phi = 50\%$. The distributions in Fig. 6(a) and (b) are shown as induced by the loading defined by Eq. (12) at $t = 400\,s$ and for one 2D cross-section of the 3D model. To facilitate comparison the same colour coding is set in Fig. 6(a) and (b). As seen in both cases, stiffness mismatch between binder and filler results in strain localisations in the binder phase. The magnitude and size of those localisations change significantly with ϕ; namely, for the case of $\phi = 10\%$ where strains localizing around filler particles may exceed the global one, applied on the macroscale, by approximately a factor of two. Significantly higher local strains are observed in case of $\phi = 50\%$. Local stresses and strain distributions obtained from the model may then be used to calculate $G(t)$ as well as $G^*(\omega)$ and $\delta(\omega)$ of the mastic, following the procedure described above, cf. Eqs. (11) and (13) to (17).

In order to validate the developed model, the stiffness ratios $G^*_{mastic}(\omega)/G^*_{bitumen}(\omega)$ are reported in Fig. 7 as obtained with the generalised self-consistent scheme (GSCS) and with the proposed FEM model for single sized spherical filler particles with 63 μm diameter. The GSCS has been reported to predict asphalt mastic properties well for low and medium volume fractions of filler [6,15]. The detailed derivation and equations for the GSCS were described by Christensen and Lo [12]. Results in Fig. 7(a) and (b) are presented for mastics with bitumen and PmB binders respectively. As seen in Fig. 5, stiffening ratios obtained with the GSCS and the FEM modelling are in very close agreement for low volume fractions of filler $\phi = 10\%$. However, the discrepancy between the results increases with increasing filler content. In particular, at $\phi = 50\%$, the differences become quite significant. The discrepancy may be attributed to stronger particles-to-particle interaction effects at higher concentrations, not accounted for by the GSCS approach, cf. [6]. Another possible explanation is the effect of filler size distribution, as the GSCS only accounts for filler volume concentration. Furthermore, as presented in Fig. 7(a) and (b) for the GSCS results obtained at $\phi = 50\%$, the calculated stiffening ratio tends to increase sharply at $\omega < 10^{-1}$ rad/s. This increase is due to convergence difficulties inherent to GSCS at high contrast between the stiffness values for the filler particles and matrix. In particular, no solution could be found with the GSCS approach for PmB binder and $\omega < 0.003$ rad/s.

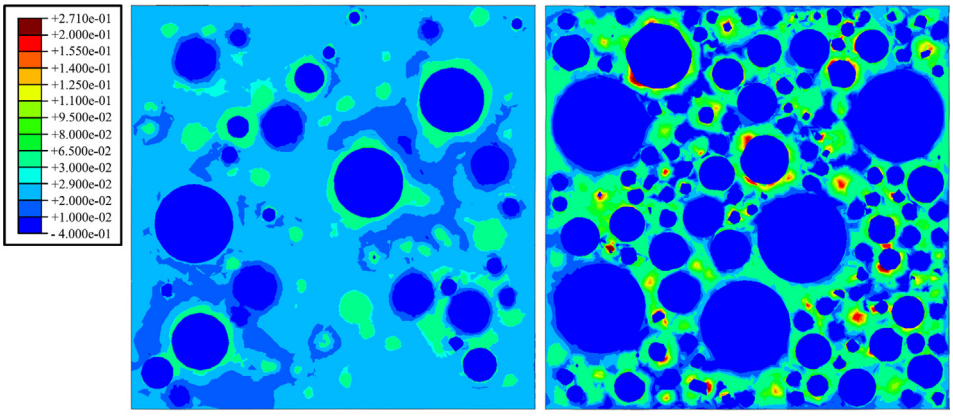

Fig. 6. A cross-section illustrating the localised ε_{33} distribution for the model with (a) ϕ =10% and (b) ϕ =50%, both models have three sizes of quartz particles mixed with bitumen 70/100.

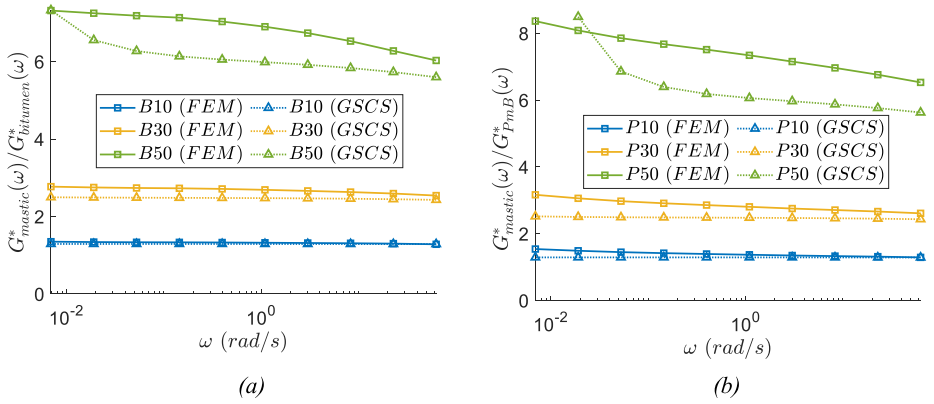

Fig. 7. Stiffening ratios comparison between the finite element simulation and the generalised self-consistent scheme (GSCS) for mastic of (a) bitumen (b) polymer-modified bitumen.

As discussed above, the modelling approach proposed in this study allows for accounting for the effect of filler size distribution on the viscoelastic properties of mastic. In order to examine this effect quantitatively, the stiffening ratios obtained with a single size filler as well as measured particle distributions for quartz sand and hydrated lime were calculated. The results are presented in Fig. 8(a) and (b) for $\phi = 30\%$ and $\phi = 60\%$ respectively. As shown in Fig. 8, the stiffening ratio at a given concentration is higher for the single size filler than for hydrated lime (HL) and quartz sand fillers (Q). The effect of filler size distribution on the stiffening ratio depends on filler concentration, as seen in Fig. 8(a) at $\phi = 30\%$; stiffening ratios obtained at different filler size distributions are within 10% from each other. This may be compared to the differences up to 40% obtained at $\phi = 60\%$. This is in line with observations reported by [36] as the particles interactions and their effect on materials stiffness is more sensitive to the actual microstructure at higher particle concentrations.

In summary, results presented in Figs. 7 and 8 show that while at low ϕ the analytical solutions of GSCS and the FEM model agree well, they start to deviate at $\phi > 30\%$. Furthermore, numerical

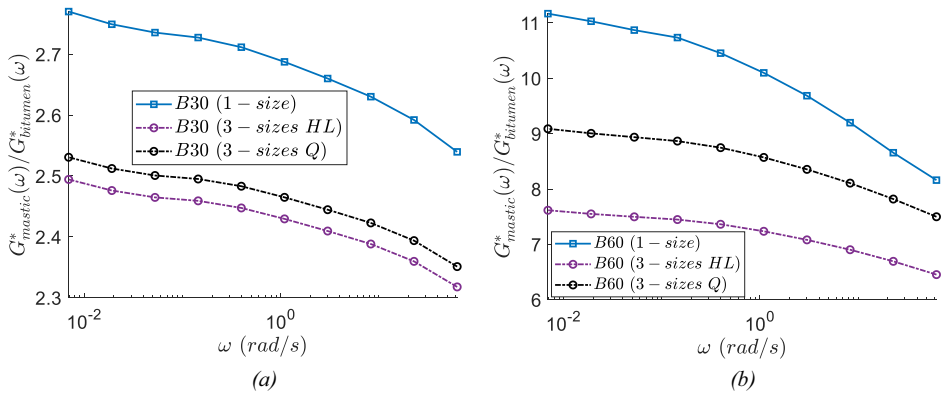

Fig. 8. Comparison of mastics stiffening ratio for the 1-size spheres model and 3-sizes spheres model as well as the GSCS at (a) $\phi = 30\%$, (b)$\phi = 60\%$.

results in Fig. 8, indicate that filler size distribution may influence the rheology of mastic significantly.

5.2. DSR measurements on mastics

Regarding the evaluation of the developed modelling approach for predicting the viscoelastic properties of mastic, in Figs. 9 and 10, the $G^*(\omega)$ measured for the four mastic materials used in this study are presented. Expectedly, the stiffening effect of hydrated lime is significantly higher as compared to the quartz sand. This is mainly due to the difference in the morphologies of the fillers, as reflected by their Rigden voids values, reported in Table 1. As previously discussed, by e.g. [28], the higher porosity of the hydrated lime results in the increased amount of binder trapped in the filler particle pores, thus stimulating the particles to form contact networks at lower ϕ. As may also be seen in Figs. 9 and 10, the frequency dependence of the mastic's $G^*(\omega)$ is somewhat reduced as compared to the respective binder. This effect is particularly pronounced at the maximum filler concentrations, i.e. at $\phi =$ 30% and 50%.

The effect of filler type and concentration on the mastic rheology is further examined in Fig. 11(a) and (b), where the stiffening ratios $G^*_{mastic}/G^*_{binder}$ are presented as a function of filler contents at frequencies $\omega = 62.8$ and 0.003 rad/s. One can see that the stiffening ratio is frequency-dependent especially at higher ϕ. For example, while the stiffening ratio of BL10 mastic increases only 18% with changing frequency from $\omega = 62.8$ to 0.003 rad/s, the corresponding increase of BL30 is 161%. Moreover, the stiffening ratios at given concentrations appear more sensitive to the filler type than the binder type for the materials and temperatures considered in this study.

5.3. Modelling predictions for viscoelastic properties of mastics

In order to capture the experimental results, reported in Figs. 9–11, mastic models as described in the previous section are used to computationally predict the $G^*(\omega)$ based on the measured complex modulus of the binder and the filler size distribution. Modelling results are shown in Fig. 12, both before and after calibration, for the hydrated lime (Fig. 12(a)) and quartz sand (Fig. 12(b)) filler size distributions. The corresponding experimental measurements are also repeated in Fig. 12 for comparison. As may be seen, the modelling results, prior to calibration, generally underestimate experimental $G^*(\omega)$ values, with the divergence between the experimental and modelling values increasing with filler content. Furthermore, the agreement for the quartz sand filler is significantly better than for the hydrated lime. This is expected, as the Rigden voids value for quartz sand reported in Table 1 is quite close to the packing density of spherical particles used in the model, cf. [37]. At the same time, the Rigden void values for the hydrated lime filler are approximately twice those for quartz sand, cf. Table 1. This is probably mainly due to differences in the filler morphologies and porosities. While this effect is not accounted for by the model in its present stage, it may be captured to a certain extent by the model calibration with the procedure described in the previous section, cf. Fig. 5 along with the pertinent discussion.

As shown in Fig. 12(a) and (b), the calibration, i.e. the simulation result at ϕ_e filler concentrations, significantly improves the model results indeed. In particular, in case of mastic with quartz sand filler, the deviations between experimental and modelling results reach at maximum 24% and are thus largely within measurements variability. At the same time, the agreement between experimental and modelling results for the hydrated lime filler is also significantly improved by calibration, the deviations between the results are somewhat higher as compared to the quartz sand and may reach 40%. It has to be emphasized, however, that the calibration procedure used presently is very simple, and as discussed in the previous section, one C_v value is determined for each binder and filler combination. In the case of bitumen binder, C_v values, identified with the calibration procedure described in the previous section, are 2.035 and 1.349 for hydrated lime and quartz sand respectively. The corresponding C_v values for PmB binder were found to be 2.187 and 1.499. Accordingly, while C_v values are strongly dependent on the filler type, they are also changing significantly with the binder type. Thus, for accurate predictions, C_v has to be determined for each binder and filler combination. It may also be pointed out, that significantly better quantitative agreement is achieved if C_v is assumed to depend on ϕ and/or T. This, however, implies a significantly more involved calibration procedure. Guo and Tan [38] have furthermore shown in their recent study that a similar filler concentration adjustment factor may be linked to filler size distribution and shape as well as to binders composition.

It has also been observed in DSR measurements that adding filler resulted in somewhat lower phase angles as compared to those measured for base binders. This effect was not particularly strong, and significant differences in phase angles were observed only for maximum filler concentrations tested, i.e. at $\phi =$ 30% and 50% for hydrated lime and quartz sand respectively. This observation is illustrated in Fig. 13, where phase angles measured for bitumen and mastic with 50% quartz sand filler are reported. Similar changes were observed for three other binder-filler combinations which are not reported here for briefness. Also in Fig. 13, $\delta(\omega)$ obtained from the mastic FEM model are presented along with the calibrated model results. Computational $\delta(\omega)$ values are

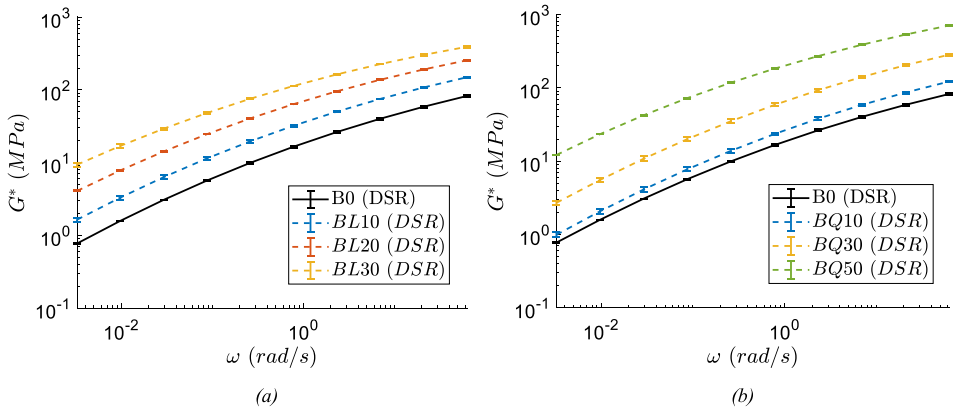

Fig. 9. Measured $G^*(\omega)$ for bitumen-filler mastics (a) hydrated lime filler, (b) quartz sand filler, the error bars represent the maximum and minimum measured values.

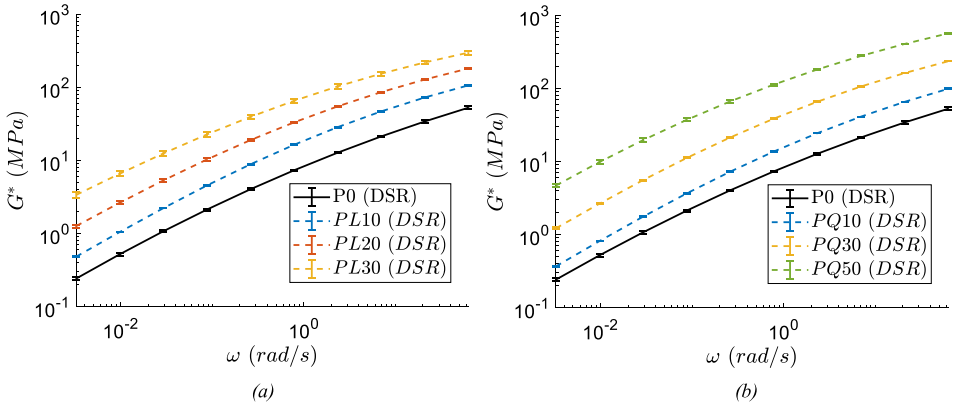

Fig. 10. Measured $G(t)$ for PmB-filler mastics (a) hydrated lime filler, (b) quartz sand filler, the error bars represent the maximum and minimum measured values.

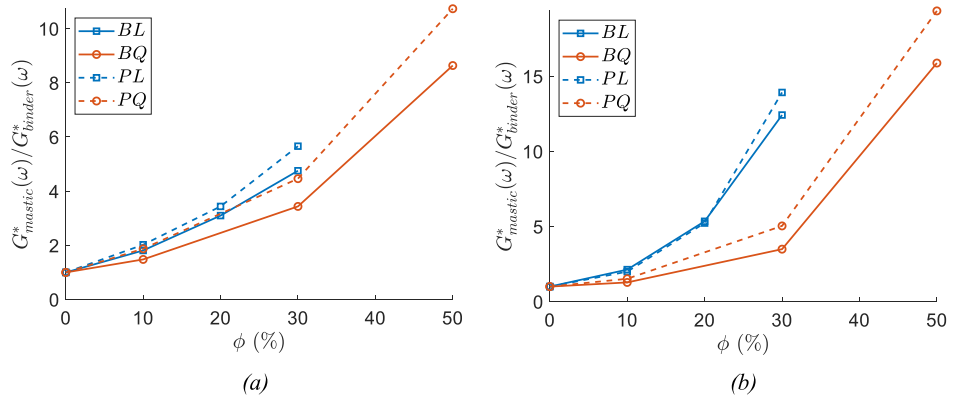

Fig. 11. Stiffening ratio for asphalt mastics (a) $\omega = 62.8\,\frac{rad}{s}$ (b)$\omega = 0.003\,\frac{rad}{s}$.

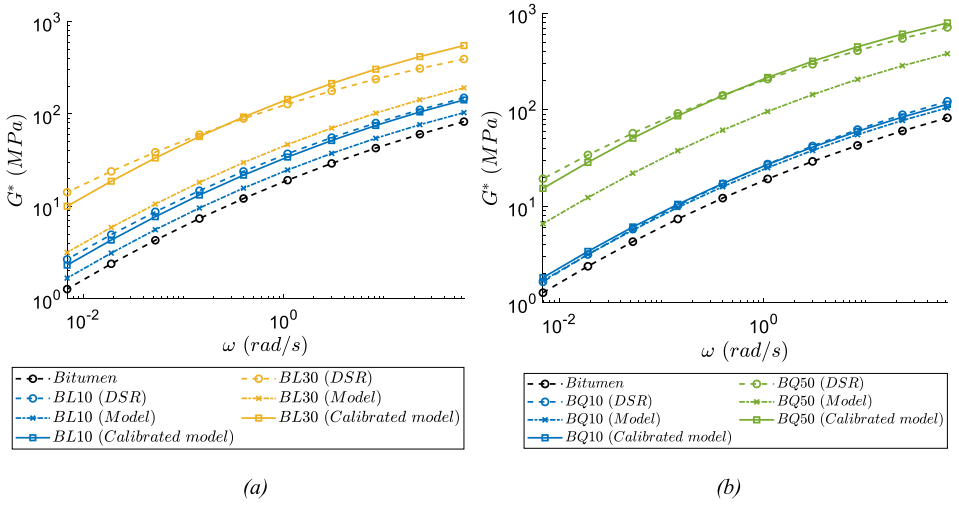

Fig. 12. Comparison between the experimental, modelled and calibrated $G^*(\omega)$ master-curves for bitumen-filler mastics (a) hydrated lime filler (b) quartz sand filler.

obtained from the calculated $G^*(\omega)$, using the Kramers-Kronig relation:

$$\delta(\omega) = 90 \cdot \frac{d\log(G^*(\omega))}{d\log(\omega)}. \tag{26}$$

As seen in Fig. 13, at $\omega > 1$ rad/s the calibrated model captures the influence of filler on $\delta(\omega)$ reasonably well. At the same time, at lower frequencies, the agreement between the measured and calculated $\delta(\omega)$ is poor, which may be attributed to the bulk behaviour, i.e. the assumption of constant $K(t)$ and its value. As illustrated in Fig. 4, the bulk behaviour has a considerable influence on the mastic behaviour at long times, which corresponds to lower measurement frequencies.

In order to further examine the model accuracy, the complex modulus values and phase angles are presented in Figs. 14 and 15 as obtained experimentally and with the developed calibrated

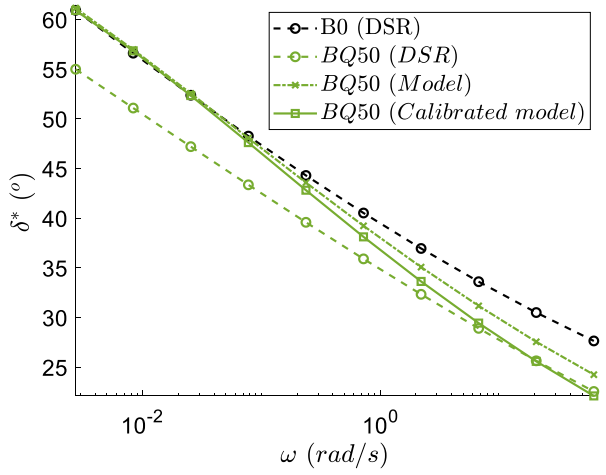

Fig. 13. Effect of the calibration procedure on the predicted phase angle.

FEM model (as illustrated in Figs. 12 and 13 above). Results in Figs. 14 and 15 are presented at $\omega = 0.003$, 10 and 62.8 rad/s for all the mastic materials. From comparing measured and predicted $G^*(\omega)$ values in Fig. 14, it is clear that the modelling approach is generally in good agreement with the experimental results. In particular, $R^2 > 0.96$ and 0.94 is found for the results reported in Fig. 14(a) and (b) respectively. The deviations between the modelling and experimental results tend to increase with decreasing ω and increasing ϕ and reach a maximum at 40%. From Fig. 15 follows that the agreement between measured and calculated $\delta(\omega)$ is also quite good, except for the case of $\omega = 0.003$ rad/s. As discussed in connection to Fig. 13 above, the deviations between modelling and experimental results in terms of $\delta(\omega)$ may partially be an artefact of the conversion procedure used for obtaining $G^*(\omega)$ and $\delta(\omega)$, from the calculated $G(t)$.

The results presented in Figs. 12–15 show that the developed FEM model captures the viscoelastic response of mastic well for all materials and temperatures examined, provided that the simulations are performed with effective filler concentrations ϕ_e. A relatively simple procedure to identify ϕ_e for each binder and filler combination is presented in Fig. 5. Moreover, the results presented in Figs. 7 and 8 demonstrate that the developed model is advantageous to the GSCS solution, as it allows accounting for filler size distribution and provides a more robust computational tool for the mastic with high ϕ and high stiffness differences between the filler and the binder, cf. Fig. 7(a) and (b). Furthermore, relying on FEM allows for a more straightforward link between mastic's macro-scale response and local stress and strain distributions in the material, cf. Fig. 6.

6. Conclusions

In this study, a new micromechanical modelling approach for predicting the viscoelastic properties of mastic was developed. The periodic boundary conditions (PBCs) were employed for the modelling of the representative volume element (RVE) of mastic and were found to be efficient for reducing the model size and improving computational efficiency. The optimal modelling

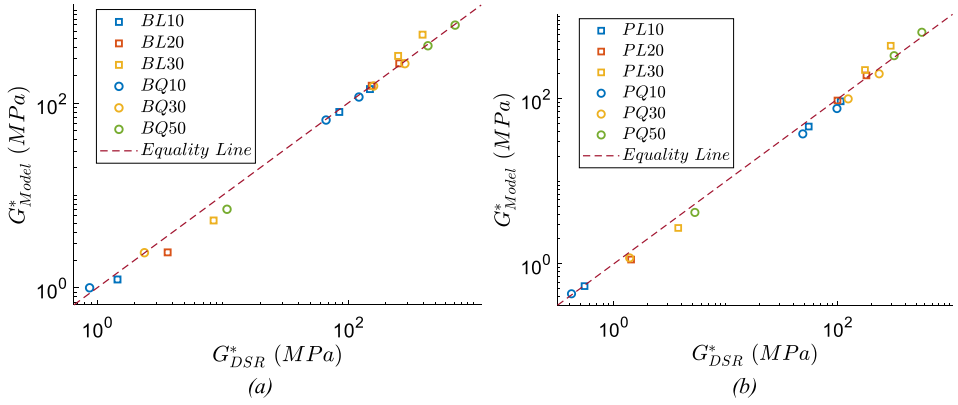

Fig. 14. $G^*(\omega)$ equality plots for mastics' experimental and modelling results (a) bitumen binder (b) PmB binder.

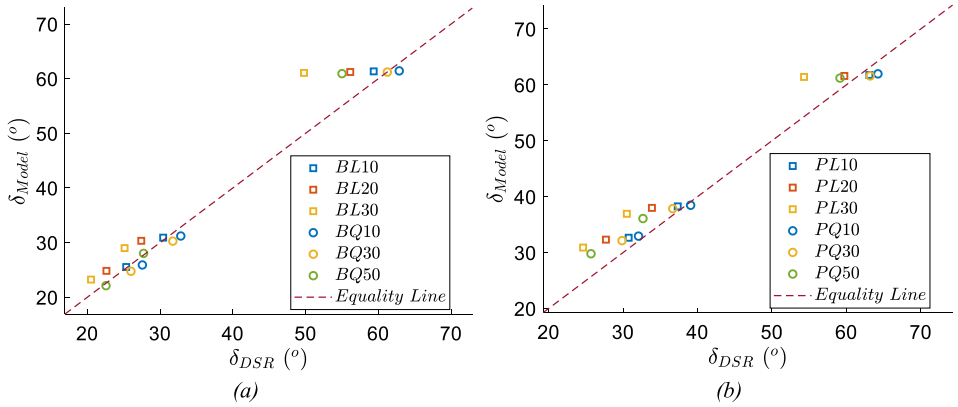

Fig. 15. $\delta(\omega)$ equality plots for mastics' experimental and modelling results (a) bitumen binder (b) PmB binder.

parameter combinations, in terms of RVE and finite element (FE) mesh sizes, were identified. Based on a brief parametric study, it was shown that a realistic description of the volumetric behaviour of the binder is crucial for the accuracy of the model. The model predictions concerning the effect of filler content on the shear relaxation modulus of mastic were compared to the Generalized Self-Consistent Scheme (GSCS) analytical solution. The numerical and GSCS solutions were found to agree well at low filler concentrations, but the difference increased with filler content. This was attributed to particle interaction effects, not captured by GSCS. It was also shown numerically, that the effect of filler size distribution on viscoelastic properties of mastic is quite significant. In particular, up to 50% change in the stiffness ratios of the mastic was observed when comparing models with different filler size distributions.

The capability of the model for capturing the viscoelastic response of mastic measured with the Dynamic Shear Rheometer (DSR) was examined for four different binder-filler combinations. The measurements were performed over a wide range of filler concentrations and for temperatures between 0 °C and 10 °C. For all mastic materials examined, it was found that the presence of filler results in both, increased complex modulus and reduced frequency dependency of the material. Accordingly, the mastic to binder stiffness ratios should be treated as frequency (or time) dependent parameters. It was shown that the model captures the measurements well, provided that the filler concentrations are adjusted in order to account for effects not incorporated into the model. A simple calibration procedure to determine the filler concentration adjustment factor for the individual binder-filler combination was proposed.

The developed modelling approach captures successfully the viscoelastic behaviour of mastic over the whole range of loading, temperature and material parameters examined. Accordingly, it may be a useful tool for optimizing mastics material design from the target viscoelastic properties. Furthermore, it is relatively straightforward for extending the FEM-based model presented in this study to the cases of non-linear material behaviour, associated e.g. with fatigue damage or plastic deformations. Thus, it potentially provides a link between mastic material design and its performance. The intention is to explore this latter aspect as a part of future studies.

CRediT authorship contribution statement

Hassan Fadil: Conceptualization, Methodology, Validation, Formal analysis, Investigation, Writing - original draft, Visualization. **Denis Jelagin:** Conceptualization, Methodology, Writing - original draft, Writing - review & editing, Supervision, Project administration, Funding acquisition. **Manfred N. Partl:** Conceptualization, Methodology, Writing - review & editing, Supervision.

Declaration of Interests

The authors declare that they have no known competing financial interests or personal relationships that could have appeared to influence the work reported in this paper.

Acknowledgements

The authors would like to acknowledge the support of the Swedish Transport Administration (Trafikverket) for funding the project (Grant No: 2015-009). The authors would also like to thank Dr X. Lu, Nynas AB, for providing the bitumen binders used in this work.

References

[1] Test Methods and Specification Criteria for Mineral Filler Used in Hot-Mix Asphalt, The National Academies 2011 Press Washington, DC.
[2] J.S. Miller, R.N. Traxler, Some of the fundamental physical characteristics of mineral filler intended for asphalt paving mixtures, J. Assoc. Asph. Paving Technol. 3 (1932) 53–63.
[3] P.J. Rigden, The use of fillers in bituminous road surfacings. A study of filler-binder systems in relation to filler characteristics, J. Soc Chem. Ind. (1947), https://doi.org/10.1002/jctb.5000660902.
[4] M. Guo, Y. Tan, L. Wang, Y. Hou, A state-of-the-art review on interfacial behavior between asphalt binder and mineral aggregate, Front. Struct. Civ. Eng. 12 (2018) 248–259, https://doi.org/10.1007/s11709-017-0422-x.
[5] A. Faheem, H. Bahia, Modelling of Asphalt Mastic in Terms of Filler-Bitumen Interaction, Road Mater. Pavement Des. 11 (2012) 281–303, https://doi.org/10.1080/14680629.2010.9690335.
[6] W.G. Buttlar, D. Bozkurt, G.G. Al-Khateeb, A.S. Waldhoff, Understanding Asphalt Mastic Behavior Through Micromechanics, Transp. Res. Rec. J. Transp. Res. Board. 1681 (2007) 157–169, https://doi.org/10.3141/1681-19.
[7] M. Guo, A. Bhasin, Y. Tan, Effect of mineral fillers adsorption on rheological and chemical properties of asphalt binder, Constr. Build. Mater. 141 (2017) 152–159, https://doi.org/10.1016/J.CONBUILDMAT.2017.02.051.
[8] J.-S. Chen, P.-H. Kuo, P.-S. Lin, C.-C. Huang, K.-Y. Lin, Experimental and theoretical characterization of the engineering behavior of bitumen mixed with mineral filler, Mater. Struct. 41 (2008) 1015–1024, https://doi.org/10.1617/s11527-007-9302-5.
[9] A. Faheem, H. Wen, L. Stephenson, H. Bahia, Effect of mineral filler on damage resistance characteristics of asphalt binders, in: Asph. Paving Technol. Proc. Tech. Sess., Publisher: Association of Asphalt Paving Technologists (AAPT), 2008: pp. 885–907. https://trid.trb.org/view/891108 (accessed September 18, 2019).
[10] H. Wang, I.L. Al-Qadi, A.F. Faheem, H.U. Bahia, S.-H. Yang, G.H. Reinke, Effect of mineral filler characteristics on asphalt mastic and mixture rutting potential, Transp. Res. Rec. J. Transp. Res. Board. 2208 (2011) 33–39, https://doi.org/10.3141/2208-05.
[11] R. Miró, A.H. Martínez, F.E. Pérez-Jiménez, R. Botella, A. Álvarez, Effect of filler nature and content on the bituminous mastic behaviour under cyclic loads, Constr. Build. Mater. 132 (2017) 33–42, https://doi.org/10.1016/j.conbuildmat.2016.11.114.
[12] R.M. Christensen, K.H. Lo, Solutions for effective shear properties in three phase sphere and cylinder models, J. Mech. Phys. Solids. 27 (1979) 315–330, https://doi.org/10.1016/0022-5096(79)90032-2.
[13] J. Qu, M. Cherkaoui, Fundamentals of Micromechanics of Solidss, 2007. https://doi.org/10.1002/9780470117835.
[14] H.M. Yin, W.G. Buttlar, G.H. Paulino, H. Di Benedetto, Assessment of existing micro-mechanical models for asphalt mastics considering viscoelastic effects, Road Mater. Pavement Des. 9 (2008) 31–57, https://doi.org/10.1080/14680629.2008.9690106.
[15] X. Ma, H. Chen, P. Yang, M. Xing, D. Niu, S. Wu, Assessment of existing micro-mechanical models for asphalt mastic considering inter-particle and physico-chemical interaction, Constr. Build. Mater. 225 (2019) 649–660, https://doi.org/10.1016/J.CONBUILDMAT.2019.07.227.
[16] E. Hesami, D. Jelagin, N. Kringos, B. Birgisson, An empirical framework for determining asphalt mastic viscosity as a function of mineral filler concentration, Constr. Build. Mater. 35 (2012) 23–29, https://doi.org/10.1016/J.CONBUILDMAT.2012.02.093.
[17] E. Hesami, B. Birgisson, N. Kringos, Numerical and experimental evaluation of the influence of the filler-bitumen interface in mastics, Mater. Struct. Constr. (2014), https://doi.org/10.1617/s11527-013-0237-8.
[18] F. Fakhari Tehrani, J. Absi, F. Allou, C. Petit, Micromechanical modelling of bituminous materials' complex modulus at different length scales, Int. J. Pavement Eng. 19 (2018) 685–696, https://doi.org/10.1080/10298436.2016.1199879.
[19] R.A. Schapery, S.W. Park, Methods of interconversion between linear viscoelastic material functions. Part II – An approximate analytical method, Int. J. Solids Struct. 36 (1999) 1677–1699, https://doi.org/10.1016/S0020-7683(98)00060-2.
[20] I.M. Gitman, H. Askes, L.J. Sluys, Representative volume: Existence and size determination, Eng. Fract. Mech. 74 (2007) 2518–2534, https://doi.org/10.1016/J.ENGFRACMECH.2006.12.021.
[21] Z. Shan, A.M. Gokhale, Micromechanics of complex three-dimensional microstructures, Acta Mater. 49 (2001) 2001–2015, https://doi.org/10.1016/S1359-6454(01)00093-3.
[22] S. Lejeunes, S. Bourgeois, Une Toolbox Abaqus pour le Calcul de Propriétés Effectives de Milieux Hétérogènes [An Abaqus Toolbox for the Calculation of Effective Properties of Heterogeneous Media], in: 10ème Colloq. Natl. En Calc. Des Struct., 2011: pp. 1–9. https://hal.archives-ouvertes.fr/hal-00592866.
[23] R. Hill, Elastic properties of reinforced solids: Some theoretical principles, J. Mech. Phys. Solids. (1963), https://doi.org/10.1016/0022-5096(63)90036-X.
[24] H.H. Hilton, Clarifications of certain ambiguities and failings of Poisson's ratios in linear viscoelasticity, J. Elast. 104 (2011) 303–318, https://doi.org/10.1007/s10659-010-9296-z.
[25] S.W. Park, R.A. Schapery, Methods of interconversion between linear viscoelastic material functions. Part I – A numerical method based on Prony

series, Int. J. Solids Struct. 36 (1999) 1653–1675, https://doi.org/10.1016/S0020-7683(98)00055-9.
[26] Nynas AB, Nynas 70/100 Paving Grade Bitumen Specifications, 2010. https://notes.nynas.com/Apps/1112.nsf/wpds/GB_EN_Nynas_70_100/$File/Nynas_70_100_GB_EN_PDS.pdf (accessed December 7, 2018).
[27] Nynas AB, Nypol 73 Polymer Modified Bitumen Specifications, 2013. https://notes.nynas.com/Apps/1112.nsf/wpds/SE_SV_Nypol_73/$File/Nypol_73_SE_SV_PDS.pdf (accessed March 11, 2019).
[28] D. Lesueur, J. Petit, H.J. Ritter, The mechanisms of hydrated lime modification of asphalt mixtures: a state-of-the-art review, Road Mater. Pavement Des. (2013), https://doi.org/10.1080/14680629.2012.743669.
[29] V. Antunes, A.C. Freire, L. Quaresma, R. Micaelo, Influence of the geometrical and physical properties of filler in the filler–bitumen interaction, Constr. Build. Mater. 76 (2015) 322–329, https://doi.org/10.1016/J.CONBUILDMAT.2014.12.008.
[30] G. Airey, Styrene butadiene styrene polymer modification of road bitumens, J. Mater. Sci. 9 (2004) 951–959 (accessed May 29, 2019) https://link.springer.com/content/pdf/10.1023%2FB%3AJMSC.0000012927.00747.83.pdf.
[31] Crystran Ltd - Quartz Crystal (SiO2) Optical Material, (n.d.). https://www.crystran.co.uk/optical-materials/quartz-crystal-sio2 (accessed October 8, 2019).
[32] K. Wolf, Laboratory Measurements and Reservoir Monitoring of Bitumen Sand Reservoir, Stanford University, 2010. https://pangea.stanford.edu/research/srb/docs/theses/SRB_122_JUL10_Wolf.pdf.
[33] S. Maillard, C. de La Roche, F. Hammoum, C. Such, J.M. Piau, Bitumen healing investigation using a specific fracture test, Road Mater. Pavement Des. 5 (2004) 45–63, https://doi.org/10.1080/14680629.2004.9689987.
[34] H. Di Benedetto, B. Delaporte, C. Sauzéat, Three-dimensional linear behavior of bituminous materials: experiments and modeling, Int. J. Geomech. 7 (2007) 149–157, https://doi.org/10.1061/(asce)1532-3641(2007)7:2(149).
[35] A. Motamed, A. Bhasin, K.M. Liechti, Using the poker-chip test for determining the bulk modulus of asphalt binders, Mech. Time-Dependent Mater. 18 (2014) 197–215, https://doi.org/10.1007/s11043-013-9222-4.
[36] A.A. Gusev, Controlled accuracy finite element estimates for the effective stiffness of composites with spherical inclusions, Int. J. Solids Struct. 80 (2016) 227–236, https://doi.org/10.1016/J.IJSOLSTR.2015.11.006.
[37] F.A.L. Dullien, Porous media: fluid transport and pore structure., (1979) 574. https://doi.org/10.1016/0300-9467(81)80049-4.
[38] M. Guo, Y. Tan, Interaction between asphalt and mineral fillers and its correlation to mastics' viscoelasticity, Int. J. Pavement Eng. (2019) 1–10, https://doi.org/10.1080/10298436.2019.1575379.